ELSEVIER

Physica D 168–169 (2002) 10–22

PHYSICA D

www.elsevier.com/locate/physd

Front explosion in a resonantly forced complex Ginzburg–Landau system

Christopher Hemming, Raymond Kapral*

Chemical Physics Theory Group, Department of Chemistry, University of Toronto, Toronto, Ont., Canada M5S 3H6

Abstract

Periodically forced oscillatory reaction–diffusion systems near the Hopf bifurcation can be modeled by the resonantly forced complex Ginzburg–Landau equation. In the 3:1 resonant locking regime this equation has three stable fixed points corresponding to the phase-locked states in the underlying reaction–diffusion system. Phase fronts separate spatial domains containing the phase-locked states. When the Ginzburg–Landau equation parameters lie in the Benjamin–Feir-unstable regime, the phase fronts have a turbulent internal spatio-temporal structure. As the forcing intensity is changed, the intrinsic width of a front grows until, at a critical value, the front "explodes" and the turbulent interfacial zone expands to fill the entire domain. The scaling properties of this transition are explored and it is shown that front width and spatial and temporal correlations diverge as the critical forcing intensity is approached. These results are compared with similar behavior seen in a coupled map model with period-3 local dynamics. The prospects for observation of these phenomena in experiments on periodically forced reaction–diffusion systems are discussed.

Keywords: Reaction–diffusion systems; Resonantly forced media; Complex Ginzburg–Landau equation

1. Introduction

If an oscillatory chemical reaction with oscillation frequency ω_0 experiences a periodic external modulation of the reaction kinetics, phase locking of the oscillations may occur when the forcing amplitude is sufficiently large and the forcing frequency ω_f is sufficiently close to a rational multiple of the natural oscillation frequency, $\omega_f/\omega_0 \approx n/m$ (n, m are co-prime integers). In a system phase-locked at the n:m resonance, a stable limit cycle exists but only n different values of the phase of the oscillations are permitted. Given one such solution, $\mathbf{c}_0(t)$, the $n-1$ remaining solutions are $\mathbf{c}_0(t+2\pi k/\omega_f)$, $k=1,2,\ldots,n-1$; these are stable to phase perturbations as well as to perturbations that displace the system from the limit cycle. In a spatially distributed reaction–diffusion system patterns typically consist of spatially uniform domains locked to these solutions. The domain walls are "phase fronts" where the phase of oscillations changes rapidly; typically the dynamics of these fronts plays a central role in the spatio-temporal pattern dynamics of such systems. Spatio-temporal dynamics in resonantly forced systems has been the subject of several experimental studies [1–5].

* Corresponding author. Tel.: +1-416-978-6106; fax: +1-416-978-5325.
E-mail address: rkapral@gatto.chem.utoronto.ca (R. Kapral).

0167-2789/02/$ – see front matter © 2002 Published by Elsevier Science B.V.
PII: S0167-2789(02)00491-8

The spatio-temporal behavior of unforced oscillatory reaction–diffusion systems and their description near the Hopf bifurcation in terms of the associated complex Ginzburg–Landau (CGL) equation:

$$\frac{\partial}{\partial t}A(\mathbf{r},t) = (\mu + \mathrm{i}\nu)A - (1+\mathrm{i}\beta)|A|^2A + (1+\mathrm{i}\alpha)\nabla^2 A \tag{1}$$

have been studied in some detail [6,7]. Here the complex amplitude describing the envelope of the oscillations is denoted by $A(\mathbf{r},t)$. The CGL parameters α and β reflect the difference in diffusion coefficients of the chemical species and the amplitude dependence of the oscillation frequency, respectively. The Benjamin–Feir-unstable regime where plane wave solutions are linearly unstable is determined by the condition $1+\alpha\beta < 0$. Since the parameters μ and ν may be eliminated from Eq. (1) by the rescaling $t \to t/\mu$, $r \to r/\sqrt{\mu}$, and $A \to \sqrt{\mu}A\,\mathrm{e}^{\mathrm{i}\nu t/\mu}$, this condition is independent of μ and ν. In this Benjamin–Feir-unstable regime the system may develop complex dynamics characterized by phase or amplitude turbulence. In such turbulent regimes the tendency is for the oscillation phase at nearby spatial locations to become decorrelated in time.

The normal form of a spatially distributed system near a Hopf bifurcation with n:m resonant forcing (where $n \leq 4$) is the forced complex Ginzburg–Landau (FCGL) equation [8,9]:

$$\frac{\partial}{\partial t}A(\mathbf{r},t) = (\mu + \mathrm{i}\nu)A - (1+\mathrm{i}\beta)|A|^2A + \gamma\bar{A}^{n-1} + (1+\mathrm{i}\alpha)\nabla^2 A. \tag{2}$$

The complex conjugate of $A(\mathbf{r},t)$ is denoted by $\bar{A}(\mathbf{r},t)$ while γ is the forcing amplitude. The parameter $\nu = \omega_0 - m\omega_\mathrm{f}/n$ indicates the extent of the detuning of the forcing from the n:m resonance. This equation describes the dynamics of the complex amplitude field in a stroboscopic representation determined by multiples of the driving period $2\pi n/\omega_\mathrm{f}$. At intermediate forcing intensities, if the CGL parameters lie in the Benjamin–Feir-unstable regime, interesting dynamics may arise from the competition between the turbulence and the forcing. We study the nature of phase fronts under such conditions.

Studies of resonantly forced oscillatory systems in the Benjamin–Feir-unstable regime have generally employed Eq. (2), which may be regarded as a generic model for systems of this type. Coullet and Emilsson [10,11] investigated phase front dynamics in the $n = 2$ case. In one spatial dimension, as γ was lowered, phase fronts with constant velocity v, whose solutions may be written in the form $A(x - vt)$, underwent a Hopf bifurcation to periodic motion of the front position, followed by a period-doubling cascade to chaotic front motion. At still lower γ, a finite-sized turbulent domain formed at the phase front. In two spatial dimensions phase fronts exhibited front roughening. For $n = 1, 2, 3, 4$, stationary spatial patterns were found. Battogtokh and Browne [12] investigated front propagation in the presence of such stationary patterns.

In this article, we examine the critical properties of fronts in 3:1 resonantly forced systems. Our earlier work [13] has shown that in the Benjamin–Feir-unstable regime in two spatial dimensions regular phase fronts exist for large values of γ while rough fronts are found for lower γ values. As γ is decreased further the fronts develop turbulent internal structure and eventually the fronts "explode" and the turbulent interfacial phase fills the entire domain. In Section 2 we describe this front explosion phenomenon in detail and compare it with an analogous phenomenon seen in a coupled map lattice (CML) model. Section 3 presents a quantitative study of the scaling properties of the front width as well as the decay constants of spatial and temporal correlation functions for the FCGL system. This section also outlines a description of the process in terms of a model of the dynamics involving two coupled interfacial profiles introduced in the study of the CML front dynamics. The conclusions of the investigation are given in Section 4.

2. Turbulent phase fronts

We present an overview of the dynamics of phase fronts seen in the 3:1 FCGL system and compare the phase front phenomenology with that observed in a CML model with period-3 local dynamics. In the simulations of

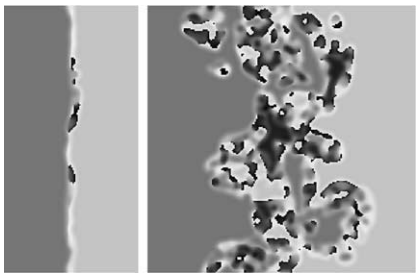

Fig. 1. Interfaces in the 3:1 FCGL for $\gamma = 0.475$ (left frame) and $\gamma = 0.459$ (right frame). The system size transverse to the front is $L = 800$. In this and subsequent figures the gray shade indicates the phase ϕ of the complex field $A = Re^{i\phi}$. Simulations were conducted in a frame moving with the front, with periodic boundary conditions on the top and bottom edges and no-flux boundary conditions on the other edges. The system size in the direction of front motion was adjusted depending on γ to be sufficiently large to contain the interface.

the FCGL equation, we fixed the parameters $\mu = 1.0$, $\nu = 1.55$, $\alpha = -1.3$ and $\beta = 1.5$. For this choice of parameters the system is obviously in the Benjamin–Feir-unstable regime for $\gamma = 0$ and supports spatially uniform 3:1 resonantly locked states for sufficiently large γ. We have not investigated other values in the CGL parameter space but phenomena similar to those described below are expected to exist where the these conditions are satisfied. The forcing intensity γ was varied to explore the front explosion process.

2.1. Fronts in the 3:1 FCGL system

In the 3:1 FCGL model there are three fixed points, which we denote A, B and C, corresponding to the three distinct resonantly locked phases in a stroboscopic representation of the dynamics in multiples of the driving period. In the reaction–diffusion system whose stroboscopic dynamics is modeled by the FCGL equation, these three phases cycle in the order A $\rightarrow$ B $\rightarrow$ C $\rightarrow$ A. We consider two-dimensional geometries with the system infinitely extended along the x-direction and periodic with length L in the y-direction. If we then suppose the left domain $x < 0$ contains phase A and the right domain $x \geq 0$ contains phase B, a phase front AB separating the A and B phases will develop and propagate from left to right. Let v_f be the mean velocity of the front. Similar interfaces BC and CA can be established between the (B,C) and (C,A) fixed-point pairs, and all such fronts propagate with the same mean velocity v_f since they are equivalent under the dynamics.

In a large parameter domain the front separating two phases is characterized by a steep but smooth variation of the phase of the complex amplitude from one phase to the other. If the CGL parameters are chosen to lie in the Benjamin–Feir-unstable regime, more complex dynamics is observed in the interfacial zone for sufficiently small forcing intensities. Examples of the complex interfacial structure are shown in Fig. 1.[1] One can see in these figures that there is no longer a smooth passage from one phase to the other as the interfacial zone is crossed; instead, complicated dynamics is seen in this zone. The intrinsic thickness of the interfacial zone may be determined by choosing left and right marker values of the complex amplitude field that delimit this zone. Let $h_L(y,t) = \min(x)$ at coordinate y where $|A(x,y,t) - A_0^L| \geq \epsilon$. Similarly, $h_R(y,t) = \max(x)$ at coordinate y where $|A(x,y,t) - A_0^R| \geq \epsilon$. Here A_0^L and A_0^R are the complex amplitude fields in the two mode locked states that the front separates and ϵ is small numerical value. We shall call $h_L(y,t)$ and $h_R(y,t)$, respectively, the left and right profiles. The instantaneous intrinsic thickness of the interfacial zone at position y along the front is then given by $\Delta(y,t) = h_R(y,t) - h_L(y,t)$.

[1] Numerical integration of the FCGL equation was performed using explicit forward differencing with discretization step sizes $\Delta x = 0.25$, $\Delta t = 0.005$. A nine point discrete Laplacian with fourth-order accuracy was used. Lengths and times are reported in the absolute space and time units in which Eq. (2) is written, with the exception of system sizes L which are reported in lattice units.

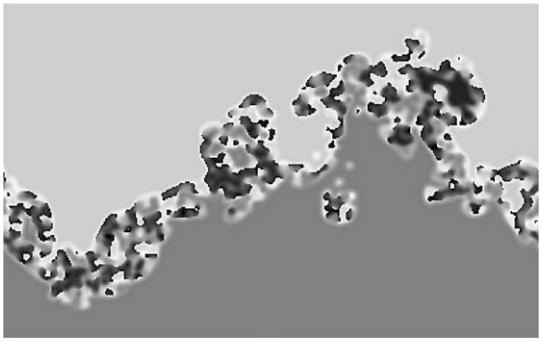

Fig. 2. The turbulent front for a larger system size, $L = 1600$, for $\gamma = 0.462$. The figure shows the variations in the shape of the front along the transverse direction as well as the variations in the intrinsic thickness of the front. (The frame has been rotated by 90° compared to Fig. 1 to accommodate the larger system size.)

Fig. 2 shows the turbulent front for a larger system size. The variations in $\Delta(y, t)$ with y are clearly visible in this figure.

The spatial average $\langle\Delta\rangle(t)$ of the intrinsic thickness may be computed from

$$\langle\Delta\rangle(t) = \frac{1}{L}\int_0^L \mathrm{d}y\, \Delta(y, t), \tag{3}$$

where, henceforth, the angle brackets will refer to an average along y. After a transient time, the phase front dynamics is observed to enter a statistically stationary regime where its average properties are independent of time, so that, for example, for sufficiently large L the average width $\langle\Delta\rangle(t) = \Delta_0$ is independent of time and depends only on the FCGL parameters. The evolution of the intrinsic width of the front starting from planar initial conditions is shown in Fig. 3. One sees that the width grows and saturates at a finite value about which it fluctuates. While the saturated width Δ_0 is independent of time it is a function of the forcing amplitude and increases as γ decreases as can be seen in the figure.

When the forcing amplitude γ is sufficiently small, less than a critical value γ^*, a finite interfacial zone can no longer be maintained and the front "explodes". The dynamics of the front in this regime is shown in Fig. 4: there are now two counter-propagating fronts where the turbulent phase consumes the each of the two mode locked phases so that asymptotically the turbulent phase fills the entire domain. The turbulent phase that exists for $\gamma < \gamma^*$ is a deterministically chaotic phase characterized by a positive Lyapunov exponent [13].

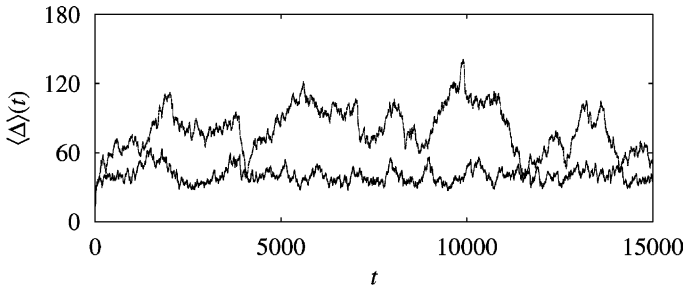

Fig. 3. Time evolution of the intrinsic width $\langle\Delta\rangle(t)$ starting from a planar front. Forcing intensity: $\gamma = 0.468$ (lower curve), $\gamma = 0.46$ (upper curve). System size: $L = 800$.

Fig. 4. Evolution of an exploding interface in the 3:1 FCGL for $\gamma = 0.454$, $t = 1000$ (left frame) and $t = 3000$ (right frame). The arrows denote the directions in which the two fronts propagate. System size: $L = 800$.

2.2. Fronts in a period-3 CML

A qualitatively similar phenomenon, where there is a progression from regular fronts, to rough fronts, to an interfacial zone with turbulent dynamics whose width diverges as parameters are tuned, has been observed in a CML with period-3 local dynamics [14]. The CML system that exhibits this phenomenon is

$$z_{n+1}(\mathbf{r}) = (1 - 4\epsilon) f(z_n(\mathbf{r})) + \epsilon \sum_{\mathbf{r}' \in \mathcal{N}_\mathbf{r}} f(z_n(\mathbf{r}')), \tag{4}$$

where

$$f(z) = \begin{cases} bz & \text{for } 0 \le z \le 1/b, \\ a & \text{for } 1/b < z \le 1 \end{cases} \tag{5}$$

and $\mathcal{N}_\mathbf{r}$ is the von Neumann neighborhood of $\mathbf{r}$. The map $f(z)$ possesses the super-stable 3-cycle solution $\mathrm{A} = a \to \mathrm{B} = ab \to \mathrm{C} = ab^2 \to \mathrm{A} = a$ and thus the system may be regarded as an abstract model for a 3:1 resonantly forced oscillatory reaction–diffusion system. The discrete points on the cycle are fixed points in a stroboscopic representation taking every third iterate of the map.

Using a system geometry and boundary conditions similar to that for the FCGL model, one may choose initial conditions to produce a front between any two of the three map fixed points as described earlier. Taking initial conditions appropriate for an AB phase front between phases A and B of the cycle and viewing the dynamics every third iterate of the CML yields a propagating front moving to the right where phase A consumes phase B. The dynamics of the front may be studied as a function of the coupling strength ϵ and the map parameters a and b. In particular, if one considers the behavior along the line $(a = 0.1, \epsilon = 0.173)$ in the (a, b, ϵ) space one observes dynamics that resembles that seen in the FCGL system; as b increases the front separating the two phases shows complex spatio-temporal structure (see Fig. 5); the intrinsic width of the interfacial zone increases until at a critical value of $b = b^*$ the width diverges and the turbulent phase fills the entire domain (see Fig. 6).

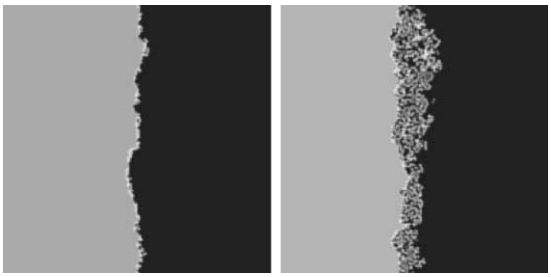

Fig. 5. Interfacial structure in the CML system equation (4) for $b = 2.45$ (left frame), $b = 2.545$ (right frame). The gray scale indicates the value of the order parameter $z_n(\mathbf{r})$. System size: 200×200.

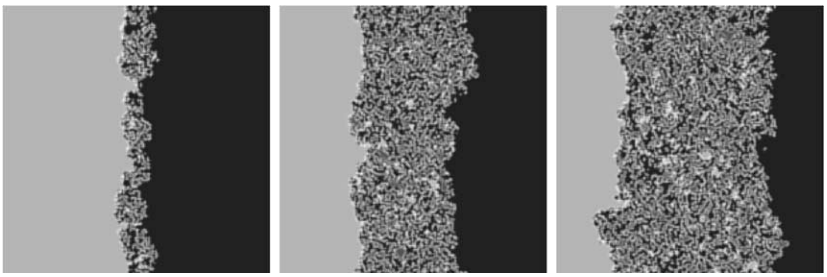

Fig. 6. Exploding front in the CML system equation (4) for $b = 2.548$ and $n = 599, 1199, 1799$ (left, middle and right frames). The gray scale indicates the value of the order parameter $z_n(\mathbf{r})$. System size: 200×200.

The CML model dynamics possesses some features that differ from those of the FCGL system. The complex interfacial dynamics is transient in nature although the transient time $\tau_{\rm tr}$ depends super-exponentially on the system size: $\tau_{\rm tr} \sim \exp(cL^{3/2})$ for systems with two spatial dimensions [14]. In this transient regime the front structure shows statistically stationary properties so that a statistical mechanical description can be carried out. Consequently, the transient behavior is the relevant behavior to study for large system sizes since the asymptotic periodic attractor will never be seen for the times of interest. The final periodic attracting state may have periods ranging from period-3 to very high periods and the attractor reached depends on the initial condition [14].

The other main difference concerns the nature of the turbulent phase. In the CML model one may show that the turbulent phase which fills the entire domain after the front explodes is characterized by a negative Lyapunov exponent even though it possesses many other characteristics of deterministic chaotic dynamics such as rapid decay of correlations. This type of dynamics has been termed *stable chaos* [15] and its properties have been studied [14–16].

As well as these differences in phenomenology, there are a number of points of difference between the two models themselves that are worth noting. The CML, being a discrete time, discrete space system, does not possess the neutral modes associated with continuous time evolution and spatial translation. The parameter ϵ in the CML represents a diffusive coupling strength, but the parameter b is not simply related to the parameters of a resonantly forced system. Indeed, the CML is an abstract system which does not directly describe any physical 3:1 forced system. Its use as a model arises from the presence of a discrete period-3 attractor, which reflects the broken time translation symmetry of the resonantly forced system, and a nonlinearity which gives rise to complex dynamics at the interface between the period-3 states. These common features may account for the similarity in the gross phenomenology of the two systems.

We now turn to a quantitative analysis of the interfacial dynamics leading to the front explosion.

3. Analysis of the front explosion

The results presented above show that the phase fronts in the FGGL and CML systems contain a turbulent zone where the dynamics of the complex amplitude field is not simply periodic. It is convenient to analyze the dynamics of fronts with complex internal structure by supposing that the turbulent zone constitutes a distinct turbulent phase, T, separated from the resonantly locked phases by the left and right profiles, $h_{\rm L}$ and $h_{\rm R}$, respectively, defined earlier. The essential elements of the structure of such phase fronts are shown in Fig. 7. Consequently, one may consider the phase front as a type of compound front composed of two interfacial profiles: one separating phase A from phase T, and the other separating phase T from phase B.

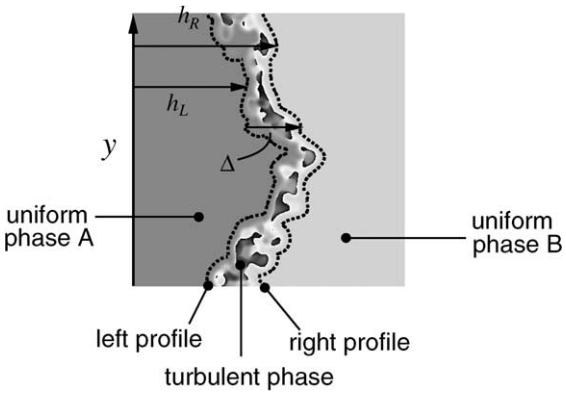

Fig. 7. Picture of the phase front in the FCGL system separating homogeneous domains of two resonantly locked phases. The turbulent zone T is delimited by left and right profiles, h_{L} and h_{R}, respectively.

Given the structure of the front shown in Fig. 7, if one wishes to study its scaling structure and determine to what extent it behaves like a diffusively rough front, one may choose to examine the dynamics of the either the left or right profiles, or the mean profile defined by $h_{\mathrm{m}} = (h_{\mathrm{R}} + h_{\mathrm{L}})/2$. The widths of the left and right profiles (not to be confused with the intrinsic width Δ) are defined as

$$w_{\mathrm{L(R)}}(t) = \langle (h_{\mathrm{L(R)}}(y,t) - \langle h_{\mathrm{L(R)}} \rangle)^2 \rangle^{1/2}, \tag{6}$$

where, as earlier, the angle brackets denote a spatial average along y. The width of the mean profile w_{m} may be defined in an analogous way by replacing $h_{\mathrm{L(R)}}$ by h_{m}. Since $h_{\mathrm{L(R)}} = h_{\mathrm{m}} \pm \Delta/2$, the width functions are related by

$$w^2_{\mathrm{L(R)}}(t) = w^2_{\mathrm{m}}(t) \pm \langle (h_{\mathrm{m}}(y,t) - \langle h_{\mathrm{m}} \rangle)(\Delta(y,t) - \langle \Delta \rangle) \rangle + \langle (\Delta(y,t) - \langle \Delta \rangle)^2 \rangle. \tag{7}$$

Because the fluctuations in the intrinsic width are independent of the system size L, if cross-correlations are neglected (these should be small for large L) one has $w_{\mathrm{R}}(t) = w_{\mathrm{L}}(t) = w_{\mathrm{m}}(t)$. Our simulation studies of the dynamics of $h_{\mathrm{L(R)}}$ show that both of these profiles satisfy Kardar–Parisi–Zhang (KPZ) scaling, provided γ is sufficiently small so that the fronts are not too thin [13]. More specifically, starting from a planar profile, the ensemble average width $w(t)$ grows as $w(t) \sim t^{\hat{\beta}}$, and saturates at $w_{\mathrm{sat}} \sim L^{\hat{\alpha}}$. The scaled width function $w(t)/L^{\hat{\alpha}}$ plotted versus $t/L^{\hat{\alpha}/\hat{\beta}}$ should be independent of the system size. The FCGL width data collapse onto a single curve if the exponents are taken to be $\hat{\alpha} = 1/2$ and $\hat{\beta} = 1/3$ [13]. These are the KPZ exponents [18].

An analogous study of the turbulent fronts in the period-3 CML model [14,16] showed that the profiles satisfied Edwards–Wilkinson (EW) [19] rather than KPZ scaling. Estimates of the importance of the nonlinear terms in the KPZ equation indicated that system sizes much larger than those used in the CML simulations would be needed to observe the KPZ scaling regime.

Since the front, although complex, maintains its integrity provided $\gamma > \gamma^*$, correlations must exist within the turbulent interfacial zone so that the A and B phases can communicate with each other. As a result it is of interest to study the structure of the interfacial zone in more detail. For this purpose we consider the dynamics of the complex amplitude field averaged along contours within the interfacial zone. We define contours $\mathbf{R}_{\mathrm{L(R)}}(t)$ located respectively near the left (right) profile and $\mathbf{R}_{\mathrm{m}}(t)$ equidistant from the left and right profiles as

$$\mathbf{R}_{\mathrm{L}}(t) = (h_{\mathrm{L}}(y,t) + 0.1\Delta(y,t), y), \tag{8}$$

$$\mathbf{R}_{\mathrm{R}}(t) = (h_{\mathrm{R}}(y,t) - 0.1\Delta(y,t), y), \tag{9}$$

$$\mathbf{R}_{\mathrm{m}}(t) = (h_{\mathrm{m}}(y,t), y). \tag{10}$$

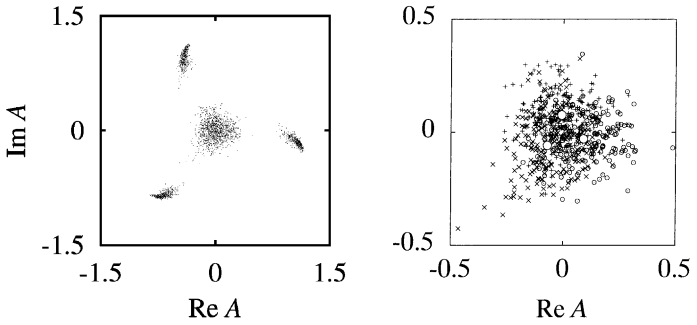

Fig. 8. Plots of the trajectories of $\langle A\rangle_{\mathrm{L}}(t)$ and $\langle A\rangle_{\mathrm{m}}(t)$ in the complex plane for the three different front types. For each simulation system size was $L = 800$ and data were collected for 4000 time units. Left panel: three outer groups of points, $\langle A\rangle_{\mathrm{L}}(t)$; central groups of points, $\langle A\rangle_{\mathrm{m}}(t)$. Right panel: magnification of the central groups of points. The three symbols correspond to the three different front types. The three large hollow circles indicate the centers of mass of the three clusters.

The averages of the $A(x, y, t)$ field over these contours are

$$\langle A\rangle_{\mathrm{L(R)}}(t) = \left(\int_{\mathbf{R}_{\mathrm{L(R)}}} \mathrm{d}s\right)^{-1} \int_{\mathbf{R}_{\mathrm{L(R)}}} \mathrm{d}s\, A(\mathbf{R}_{\mathrm{L(R)}}, t), \tag{11}$$

$$\langle A\rangle_{\mathrm{m}}(t) = \left(\int_{\mathbf{R}_{\mathrm{m}}} \mathrm{d}s\right)^{-1} \int_{\mathbf{R}_{\mathrm{m}}} \mathrm{d}s\, A(\mathbf{R}_{\mathrm{m}}, t), \tag{12}$$

where s is the arc length along the contours.

Fig. 8 (left panel) shows the time evolution of $\langle A\rangle_{\mathrm{L}}(t)$ and $\langle A\rangle_{\mathrm{m}}(t)$ from simulations of the three different front types, AB, BC and CA. (The $\langle A\rangle_{\mathrm{R}}(t)$ results contain the same information as the corresponding left profile results.) A simulation of the FCGL equation for a given front type, say AB, will yield one of the outer groups of points for $\langle A\rangle_{\mathrm{L}}(t)$ since the FCGL equation gives a stroboscopic representation of the dynamics. The other two outer groups of points are obtained from simulations of the other two front types. Since there is no overlap between these groups, the average field on this contour maintains phase coherence. The $\langle A\rangle_{\mathrm{m}}(t)$ values for the three front types comprise the center group of points in this figure. Fig. 8 (right panel) shows a magnification of this group. Although there is considerable overlap of the three clusters of points, their centers of mass are separated. Consequently, along this center contour, although there is a breakdown of phase coherence, phase coherence is partially maintained as indicated by the separation between the centers of mass.

It is also of interest to study the $A(x, y, t)$ field averaged over the entire interfacial zone; let

$$\langle A\rangle_{I}(t) = (L\langle\Delta\rangle(t))^{-1} \int_0^L \mathrm{d}y \int_{h_{\mathrm{L}}(y,t)\le x\le h_{\mathrm{R}}(y,t)} \mathrm{d}x\, A(x, y, t). \tag{13}$$

The time evolution of this quantity is shown as a phase plane plot in Fig. 9. One can see that the three groups of points do not overlap indicating that spatially averaged dynamics in the interfacial zone maintains phase coherence. The centers of mass of these groups tend to zero as $\gamma \to \gamma^{*+}$ so that phase coherence between the two homogeneous phases is destroyed at the transition point. This feature is also seen in the spatially averaged dynamics of the A field along the $\mathbf{R}_{\mathrm{m}}$ contour.

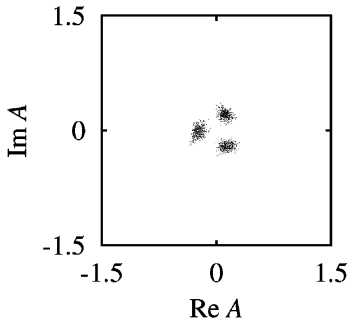

Fig. 9. Phase plane plot of $\langle A\rangle_I(t)$. The three groups of points correspond to the three interface types. For each simulation system size was $L = 800$ and data were collected for 4000 time units.

3.1. Scaling properties

We next quantitatively characterize the manner in which the front explosion occurs in the FCGL system. Simulations show that two processes occur simultaneously as the front explodes: the mean velocity of the front tends to zero and the width of the front diverges.

We define the mean intrinsic front width $\Delta_0 \equiv \langle\langle\Delta(y', t')\rangle\rangle$ where $\langle\langle\cdot\rangle\rangle$ denotes an average over space and time (y', t') in the statistically stationary regime. Fig. 10 shows how the intrinsic width Δ_0 varies with γ as the explosion transition is approached from the stable front side, $\gamma \to \gamma^{*+}$. One sees that Δ_0 diverges as $\Delta_0 \sim |\gamma - \gamma^*|^{-\alpha}$ with $\gamma^* = 0.458$ and $\alpha = 0.47$. The fluctuations in the front width $\langle\langle(\delta\Delta)^2\rangle\rangle$, where $\delta\Delta(y,t) \equiv \Delta(y,t) - \Delta_0$, also diverge as $\langle\langle(\delta\Delta)^2\rangle\rangle \sim |\gamma - \gamma^*|^{-\mu}$ where $\mu = 1.34$ and again $\gamma^* = 0.458$ (see Fig. 10, right panel). (The exponents α, β and μ introduced in this section should not be confused with the CGL parameters in Section 2.)

For γ values approaching the transition, the probability distribution $P(\delta\Delta)$ can be rescaled with good agreement to an invariant function g such that $P(\delta\Delta) = g(\delta\Delta/|\gamma - \gamma^*|^{-\kappa})/|\gamma - \gamma^*|^{-\kappa}$ by taking $\kappa = 0.65$ for $\gamma^* = 0.458$ (Fig. 11). The existence of such a universal function g requires that $\mu = 2\kappa$, since $\langle\langle(\delta\Delta)^2\rangle\rangle = |\gamma - \gamma^*|^{-2\kappa}\int_{-\infty}^{\infty} du\, u^2 g(u)$ where $u = \delta\Delta/|\gamma - \gamma^*|^{-\kappa}$. The values $\mu = 1.34$ and $\kappa = 0.65$ are approximately consistent with the relation $\mu = 2\kappa$. In the CML system, the $P(\delta\Delta)$ scaling exponent κ was equal to the intrinsic width scaling exponent $\alpha \simeq 1/3$.

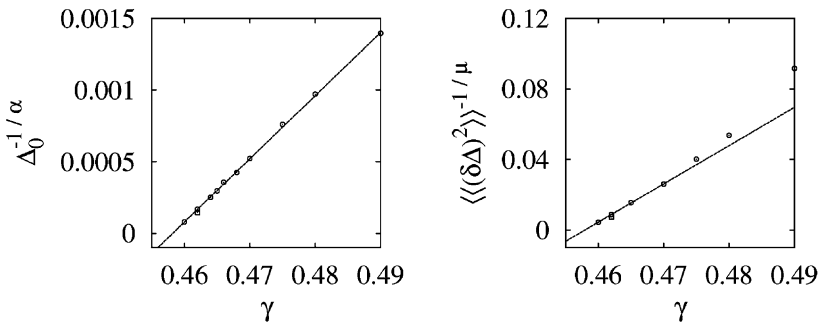

Fig. 10. Left panel: $\Delta_0^{-1/\alpha}$ versus γ (circles, square), where $\alpha = 0.47$. The dashed line is $0.04405(\gamma - 0.458)$. Right panel: dependence of $\langle\langle(\delta\Delta)^2\rangle\rangle^{-1/\mu}$ on γ, where $\mu = 1.34$. The dashed line has equation $\langle\langle(\delta\Delta)^2\rangle\rangle^{-1/\mu} = 2.170(\gamma - 0.458)$. The exponents α and μ were determined by a fit to the data for $\gamma \le 0.47$. In Figs. 10, 12 and 13 hollow circles indicate values from systems of size of $L = 800$ with average measured over intervals from 3×10^4 to 2.6×10^5 time units in length; the hollow square in each plot is a value from a system with $L = 1600$ over an interval of 6×10^4 time units.

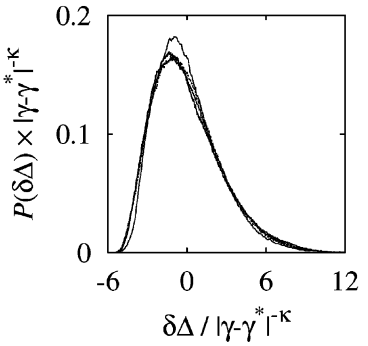

Fig. 11. Scaled $\delta\Delta$ probability distribution $P(\delta\Delta)|\gamma - \gamma^*|^{-\kappa}$ versus $\delta\Delta/|\gamma - \gamma^*|^{-\kappa}$, where $\gamma^* = 0.458$ and $\kappa = 0.65$. The curves are for $\gamma = 0.46$ (solid), 0.462 (long dashes), 0.465 (short dashes), 0.475 (dots). Data were collected in systems of size $L = 800$ over intervals of 3.9×10^4–2.6×10^5 time units duration.

The mean velocity varies with γ and decreases to zero as $\gamma \to \gamma^{*+}$. The variation of the mean velocity v_f of the front with γ is shown in Fig. 12 where one can see that $v_f \sim |\gamma - \gamma^*|$ close enough to γ^*. The critical value of γ is found to be $\gamma^* = 0.457$ from a fit to the linear portion of the data near the critical point. The agreement between the γ^* values extracted from these measurements is in accord with the notion that the behaviors of these two properties signal the onset of the explosion transition.

Since the local fluctuations in the intrinsic width become pronounced as $\gamma \to \gamma^{*+}$ we expect that correlations in the width along y will grow. Hence, the correlation length ℓ that characterizes the decay of the correlation function

$$C_\Delta(y) = \frac{\langle\langle \delta\Delta(y + y', t')\delta\Delta(y', t')\rangle\rangle}{\langle\langle(\delta\Delta(y', t'))^2\rangle\rangle} \tag{14}$$

will diverge as the critical point is approached. The function $C_\Delta(y)$ is found to develop long range correlations as $\gamma \to \gamma^{*+}$, but it is difficult to extract the precise form of the γ dependence of ℓ accurately. Since the correlation length grows, one must simulate systems with very large transverse dimensions to ensure that correlations decay on scales smaller than the system length. In addition, the existence of short range correlations make it difficult to unambiguously extract the value of the characteristic decay length. Fig. 13 (left) plots our estimates of the correlation length ℓ as a function of γ.

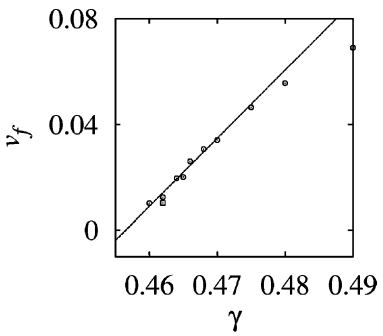

Fig. 12. The mean "center of mass" interface velocity v_f versus γ (circles, square). The long-dashed curve is a linear fit to the data for $\gamma \leq 0.47$ which yields $\gamma^* = 0.457$. The system sizes and simulation durations are described in the caption of Fig. 10.

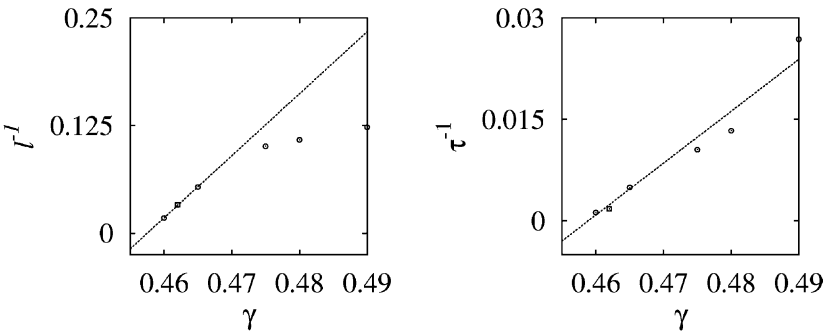

Fig. 13. Left: the reciprocal of the correlation length ℓ^{-1} versus γ (circles, square). The equation of the dashed line is $\ell^{-1} = 7.203(\gamma - 0.458)$. Right: the reciprocal of the correlation time τ^{-1} versus γ (circles, square). The equation of the dashed line is $\tau^{-1} = 0.7669(\gamma - 0.459)$. The lines are intended as guides to the eye and were obtained by a fit to the data for $\gamma \leq 0.47$. The system sizes and simulation durations are described in the caption to Fig. 10.

The temporal autocorrelation function of the intrinsic width is defined by

$$C_{\Delta}(t) = \frac{\langle\langle \delta\Delta(y', t + t')\delta\Delta(y', t')\rangle\rangle}{\langle\langle (\delta\Delta(y', t'))^2\rangle\rangle} \tag{15}$$

and its decay may be characterized by the decay constant τ which is plotted in Fig. 13 (right) as a function of γ. These qualitative data suggest that the spatial and temporal correlations of the intrinsic width diverge as $\gamma \to \gamma^{*+}$. Reliable estimates of the nature of the divergence are difficult to obtain without considerably more extensive simulations on larger systems.

The scaling structure of the front explosion was examined in considerable detail for the CML model [14,16,17]. Simulations of the CML are sufficiently efficient so that very large systems can be evolved for long time periods to determine the scaling behavior of v_{f}, Δ_0, ℓ and τ. Even for this model it is difficult to determine the γ dependence of ℓ and τ accurately. As in the FCGL simulations, the variations of both v_{f} and Δ_0 are much easier to reliably determine.

The CML simulations showed that $v_{\mathrm{f}} \sim |b - b^*|$ and $\Delta_0 \sim |b - b^*|^{-\alpha}$, where $\alpha = 1/3$, as the critical value of b is approached from the stable front side, $b \to b^{*-}$. In both the CML and FCGL systems the velocity of the front vanishes linearly with the distance from the critical value. However, the power law behavior of Δ_0 differs for these two systems since $\alpha = 1/2$ for the FCGL data presented earlier.

The scaling exponents in the CML model were calculated using a stochastic model of the dynamics that described the turbulent front in terms of a pair of coupled EW left and right profiles, h_{L} and h_{R}, moving with velocities $+v$ and $-v$, respectively, coupled by repulsive forces, F_{L} and F_{R} that depend only on $\Delta = h_{\mathrm{R}} - h_{\mathrm{L}}$:

$$\frac{\partial h_{\mathrm{R}}(y,t)}{\partial t} = \mathcal{D}\frac{\partial^2 h_{\mathrm{R}}}{\partial y^2} - v + F_{\mathrm{R}}(h_{\mathrm{R}}(y,t) - h_{\mathrm{L}}(y,t)) + \xi_{\mathrm{R}}(y,t), \tag{16}$$

$$\frac{\partial h_{\mathrm{L}}(y,t)}{\partial t} = \mathcal{D}\frac{\partial^2 h_{\mathrm{L}}}{\partial y^2} + v + F_{\mathrm{L}}(h_{\mathrm{R}}(y,t) - h_{\mathrm{L}}(y,t)) + \xi_{\mathrm{L}}(y,t), \tag{17}$$

where $\xi_{\mathrm{L(R)}}$ are Gaussian white noise terms. Assuming that the velocity v varies linearly with $|b - b^*|$, and power law decays of the forms $\Delta_0 \sim |b - b^*|^{-\alpha}$, $\ell \sim |b - b^*|^{-\beta}$ and $\tau \sim |b - b^*|^{-z}$, one finds $\alpha = 1/3$, $\beta = 2/3$, $z = 4/3$ from a scaling analysis of the coupled equations. These theoretical exponents are consistent with the measured CML values.

4. Discussion

The front dynamics and the front explosion that occurs for small forcing amplitudes in the 3:1 FCGL system when the CGL parameters lie in the Benjamin–Feir-unstable regime were shown to exhibit a rich repertoire of behavior with a number of unusual features.

The gross phenomenology of the front dynamics as the transition is approached is similar to that first observed in the super-stable period-3 coupled map lattice [14]. In particular, diffusively rough fronts in deterministic systems, whose profile widths scale like the square root of the system size, are seen in both systems. However, while KPZ scaling of the profile widths is found in the FCGL profiles, EW scaling was found in the CML profiles. The system sizes needed to enter the regime where the nonlinear terms are important were sufficiently large to preclude CML simulations in that regime. The fact that the turbulence in the CML has its origin in "stable chaos" rather than true chaos as in the FCGL system does not appear to be an essential ingredient for the front explosion or the qualitative behavior of the turbulent front dynamics.

The front explosion possesses the signatures of a non-equilibrium phase transition. The intrinsic width diverges with power law behavior and this divergence is accompanied by divergences in its spatial and temporal correlations. The scaling exponents differ from those measured for the CML system. This difference might be attributable to the differences in these systems, in particular, the nature of the correlations in the turbulent zone. However, one cannot rule out the possibility that the present calculations are too far from the transition point so that the asymptotic scaling behavior has not yet been achieved. While calculations that lie closer to the transition point than those presented in this paper are desirable, they are very difficult to carry out because of the usual problems associated with behavior near critical points. Large transverse system sizes are needed to ensure that diverging correlations decay on scales shorter than the system size, large system sizes parallel to the propagation direction are needed since the width grows as the transition is approached, and long times are needed to avoid transient behavior which also diverges. The scaling exponent for the intrinsic width is most easily measured and it shows a clear departure from the CML value. This suggests there are quantitative differences in these two systems although the gross phenomenology is similar.

While the CML is an abstract model whose connection to real systems is difficult establish, the calculations presented here on a normal form model for a reaction–diffusion system suggest that the front phenomena seen in these two systems can now be sought in experiments on resonantly forced oscillatory media. Although quantitative aspects of the front explosion might be difficult to measure in experiments on resonantly forced reaction–diffusion systems, the qualitative phenomenology exhibited by these unusual chemical fronts might be much easier to observe. The Belousov–Zhabotinsky reaction has been studied in the 3:1 resonantly forced regime [2] where rough interfaces separate pairs of the three mode locked states. Furthermore, conditions have been found where the Belousov–Zhabotinsky reaction without external forcing displays spatio-temporal turbulent dynamics [20]. Such systems under 3:1 resonant forcing might be candidates for the observation of the phenomena described in this paper.

Acknowledgements

This work was supported in part by a grant from the Natural Sciences and Engineering Research Council of Canada.

References

[1] A. Chiffaudel, S. Fauve, Phys. Rev. A 35 (1987) 4004.
[2] V. Petrov, Q. Ouyang, H.L. Swinney, Nature (London) 388 (1997) 655.

[3] V. Petrov, M. Gustaffson, H.L. Swinney, in: M. Ding, W. Ditto, L. Pecora, S. Vohra, M. Spano (Eds.), Proceedings of the Fourth Experimental Chaos Conference, Boca Raton, FL, August 6–8, 1997, World Scientific, New York, 1998.
[4] A.L. Lin, V. Petrov, H.L. Swinney, A. Ardelea, G.F. Carey, in: M. Golubitsky, D. Luss, S.H. Strogatz (Eds.), Pattern Formation in Continuous and Coupled Systems, The IMA Volumes in Mathematics and Its Applications, Vol. 115, Springer, New York, 1999, p. 193.
[5] A.L. Lin, A. Hagberg, A. Ardelea, M. Bertram, H.L. Swinney, E. Meron, Phys. Rev. E 2000 62 (2000) 3790.
[6] Y. Kuramoto, Chemical Oscillations, Waves and Turbulence, Springer, Berlin, 1984.
[7] M.C. Cross, P.C. Hohenberg, Rev. Mod. Phys. 65 (1993) 851.
[8] J.M. Gambaudo, J. Diff. Eqns. 57 (1985) 172.
[9] C. Elphick, G. Iooss, E. Tirapegui, Phys. Lett. A 120 (1987) 459.
[10] P. Coullet, K. Emilsson, Physica A 188 (1992) 190.
[11] P. Coullet, K. Emilsson, Physica D 62 (1992) 119.
[12] D. Battogtokh, D.A. Browne, Phys. Lett. A 266 (2000) 359.
[13] C.J. Hemming, R. Kapral, Faraday Disc. 120 (2001) 371.
[14] R. Kapral, R. Livi, G.-L. Oppo, A. Politi, Phys. Rev. E 49 (1994) 2009.
[15] A. Politi, R. Livi, G.-L. Oppo, R. Kapral, Europhys. Lett. 22 (1993) 571.
[16] Y. Cuche, R. Livi, A. Politi, Physica D 103 (1997) 369.
[17] R. Kapral, R. Livi, A. Politi, Phys. Rev. Lett. 79 (1997) 112.
[18] M. Kardar, G. Parisi, Y.-C. Zhang, Phys. Rev. Lett. 56 (1986) 889.
[19] S.F. Edwards, D.R. Wilkinson, Proc. Roy. Soc. Lond. A 381 (1982) 17.
[20] Q. Ouyang, J.-M. Flesselles, Nature 379 (1996) 142.